EARTHQUAKE ENGINEERING AND STRUCTURAL DYNAMICS, VOL. 25, 1307–1327 (1996)

CONSISTENT INFINITESIMAL FINITE-ELEMENT CELL METHOD IN FREQUENCY DOMAIN

JOHN P. WOLF AND CHONGMIN SONG

Department of Civil Engineering, Institute of Hydraulics and Energy, Swiss Federal Institute of Technology Lausanne, CH-1015 Lausanne, Switzerland

SUMMARY

To calculate the dynamic-stiffness matrix at the structure–medium interface of an unbounded medium for the range of frequencies of interest, the consistent infinitesimal finite-element cell method based on finite elements is developed. The derivation makes use of similarity and finite-element assemblage, yielding a non-linear first-order ordinary differential equation in frequency. The asymptotic expansion for high frequency yields the boundary condition satisfying the radiation condition. In an application only the structure–medium interface is discretized resulting in a reduction of the spatial dimension by one. The boundary condition on the free surface is satisfied automatically. The consistent infinitesimal finite-element cell method is exact in the radial direction and converges to the exact solution in the finite-element sense in the circumferential directions. Excellent accuracy results.

KEY WORDS: consistent boundary; dynamic stiffness; far field; radiation condition; soil–structure interaction; unbounded medium

1. INTRODUCTION

To analyse dynamic medium–structure interaction based on the substructure method in the frequency domain, the dynamic-stiffness matrix in the degrees of freedom on the structure–medium interface of the unbounded medium is determined. For a transient load the dynamic-stiffness matrix throughout the frequency range of interest is needed. As an alternative to the boundary-element method, which applies an analytical solution incorporating the radiation condition at infinity, the consistent infinitesimal finite-element cell method based solely on the finite-element formulation is described in this paper. For an analysis in the time domain for which the unit-impulse response matrix of the unbounded medium is calculated, the consistent infinitesimal finite-element cell method is derived for the three-dimensional vector wave equation in Reference 1.

The consistent infinitesmal finite-element cell method in the frequency domain is described in a stand-alone paper. A certain amount of duplication with Reference 1 is thus inevitable. Significant improvements in the derivation are introduced.

The concept and salient features of the consistent infinitesimal finite-element cell method are discussed in Section 2. The fundamental equations in the frequency domain are derived in Section 3, leading to a non-linear first-order ordinary differential equation in frequency. The boundary condition which is necessary to be able to start the solution procedure of the differential equation follows from an asymptotic expansion for high frequency in Section 4. Examples demonstrating the high accuracy and versatility of the consistent infinitesimal finite-element cell method are described in Section 5. Concluding remarks are stated in Section 6.

2. CONCEPT AND SALIENT FEATURES

The consistent infinitesimal finite-element cell method is a concise implementation to calculate the dynamic-stiffness matrix of the unbounded medium based on similarity and finite elements.

CCC 0098–8847/96/111307–21

Received 1 March 1996
Revised 4 June 1996

Without addressing any details, the concept of the consistent infinitesimal finite-element cell method can be described. The dynamic-stiffness matrix at the structure–medium interface of the unbounded medium is to be determined. In an application only the structure–medium interface is discretized. In the derivation of the consistent infinitesimal finite-element cell equation a fictitious similar interface with the similarity centre O at an infinitesimal distance from the actual structure–medium interface measured in the radial direction is introduced (Figure 1(a)). The similar interfaces are defined by the characteristic length r: r_i for the structure–medium interface, r_e for the fictitious interface. r_e follows from r_i as

$$r_e = (1 + w)r_i \tag{1}$$

with the infinitesimal dimensionless length w. A relationship for the dynamic-stiffness matrices of the unbounded medium at these two similar interfaces exists.

The region between the structure–medium interface and the fictitious interface is a cell of infinitesimal width which is discretized with finite elements (Figure 1(b)). Its interior and exterior boundaries coincide with the structure–medium interface and the fictitious interface, respectively. The arrangement of the nodes on the two boundaries must satisfy similarity. w in equation (1) is thus called the infinitesimal dimensionless cell width. Adding the infinitesimal finite-element cell to the unbounded medium defined by the fictitious interface (Figure 1(c)) results in the unbounded medium defined by the structure–medium interface. The same applies to their dynamic-stiffness matrices. This *assemblage enforcing compatibility and equilibrium* results in another relationship linking the dynamic-stiffness matrices at the two interfaces. Substituting the relationship based on *similarity* mentioned above permits the dynamic-stiffness matrix at the structure–medium interface to be expressed as a function of the dynamic-stiffness matrix (determined from the static-stiffness and mass matrices) of the finite-element cell. After performing the limit of the infinitesimal cell width *analytically* only the discretization on the structure–medium interfaces is present (Figure 1(a)). The resulting consistent infinitesimal finite-element cell equation is a non-linear first-order ordinary differential equation with the coefficient matrices obtained from assemblage of those of the surface finite elements on the structure–medium interface.

This concept is sufficient to discuss the salient features of the consistent infinitesimal finite-element cell method which are compared with those of the boundary-element method. In an actual calculation the discretization with surface finite elements is limited to the structure–medium interface. This results in a *reduction of the spatial dimension by one* as in the boundary-element method. But the consistent infinitesimal finite-element cell method is based solely on the finite-element formulation and does not require a fundamental solution. Any finite-element discretization can be applied. The coefficient matrices of the

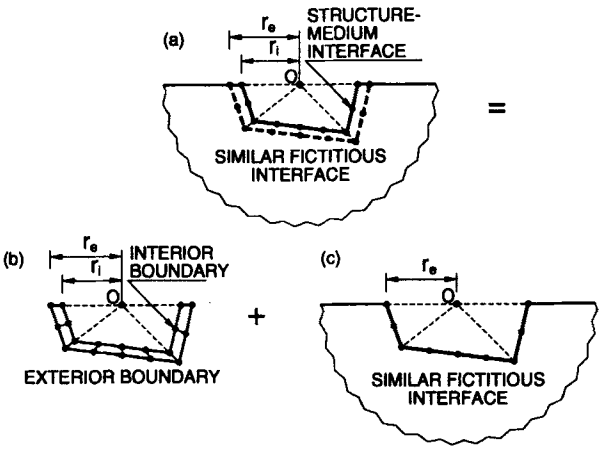

Figure 1. Concept of consistent infinitesimal finite-element cell method with infinitesimal cell width leading to finite-element discretization of structure–medium interface only

consistent infinitesimal finite-element cell equation depend on the geometry of the structure–medium interface and on the material properties of the unbounded medium. The procedure is *exact in the radial direction and converges to the exact solution in the finite-element sense in the circumferential directions.* As the discretization and the unknowns are only introduced on the boundary, the consistent infinitesimal finite-element cell method can be regarded as a boundary-element method based on finite elements called *boundary finite-element method.*

For the two-dimensional horizontally layered medium the characteristic lengths of the interior and exterior boundaries are the same. This corresponds to placing the centre of similarity at infinity. For this case the consistent infinitesimal finite-element cell method leads to a formulation identical to that of the consistent-boundary method.[2,3] However, the concept is not the same as in the consistent boundary where the analytical solution of the displacements in the radial direction must be known.

The consistent infintesimal finite-element cell method satisfies the radiation condition which is also the case for the boundary-element procedure.

As the consistent infinitesimial finite-element cell method uses polynomial shape functions as in the conventional finite-element method, the integrations are simple to perform. This is in contrast to the integrations of singular functions occurring in the fundamental solutions of the boundary-element method.

The dynamic-stiffness matrix resulting from the consistent infinitesimal finite-element cell method is symmetric. This does not apply to the results of the conventional boundary-element method where special and more complicated formulations are necessary to enforce symmetry. Symmetry is required to perform an unbounded medium–structure-interaction analysis consistently where the structure is modelled with finite elements.

The relationship based on similarity is also applicable to the inhomogeneous case compatible with similarity. An example with inhomogeneities in shear modulus G, Poisson's ratio ν and mass density ρ is shown in Figure 2. Obviously, the other relationship describing the assemblage of finite elements is also valid for inhomogeneities. Thus, the consistent infinitesmial finite-element cell method which is based on these two relationships can be used. The boundary conditions at the interfaces and at the free surface are satisfied rigorously and automatically without any further discretization. Material inhomogeneities which satisfy similarity and the boundary condition at the free surface can thus be processed without any increase in the number of degrees of freedom. In contrast, in the boundary-element method, the interfaces and the free surface must be discretized which increases the computational effort when the fundamental solution of the full space is used. In addition, on these boundaries extending to infinity truncation of the discretization has to be introduced in the boundary-element method which leads to errors. The latter are difficult to evaluate. To avoid the discretization on the free surface, the fundamental solution of the half-space could be used which is, however, much more complicated.

The consistent infinitesimal finite-element cell method based on similarity can also process materials with anisotropic behaviour and with properties varying in the radial direction as a power function straightforwardly, whereby the computational effort is hardly affected. In contrast, the fundamental solution of the boundary-element method is very complicated in the orthotropic case and does not exist in the general anisotropic case.

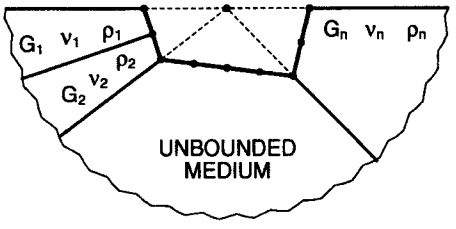

Figure 2. Unbounded medium with material inhomogeneity satisfying similarity

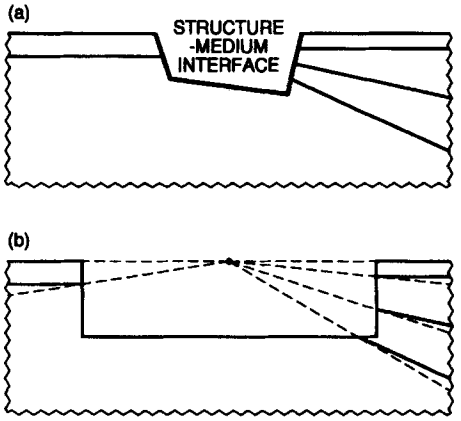

Figure 3. (a) Original dynamic unbounded medium–structure-interaction problem with layers. (b) Approximate representation enforcing similarity of unbounded medium with structure–medium interface moved outwards

The consistent infinitesimal finite-element cell method requires similarity of the unbounded medium, which is not always satisfied in practice. An example with a layered unbounded medium (Figure 3(a)) is used for illustration. By moving the structure–medium interface outwards, an approximate representation of the unbounded medium satisfying similarity (Figure 3(b)) can be constructed. The farther away the structure–medium interface is chosen, the better the approximation becomes. This procedure should be compared with that of truncating the discretization of the interfaces extending to infinity as used in the boundary-element method.

3. FUNDAMENTAL EQUATIONS

3.1. Dynamic-stiffness matrices at similar structure–medium interfaces of unbounded medium

A *dimensional analysis* is performed to identify the independent dimensionless variables of which the dynamic-stiffness matrices at similar structure–medium interfaces (Figure 1(a)) of the unbounded medium $[S^{\infty}(r, \omega)]$ (superscript ∞ for unbounded) are a function. Besides Poisson's ratio v (which is already dimensionless), the characteristic length r (which fully defines a specific structure-medium interface (Figure 1(a))), the shear modulus G, the mass density ρ and the frequency ω are sufficient to determine $[S^{\infty}(r, \omega)]$. A bracket denotes the dimension; $[L]$, $[M]$ and $[T]$ are the dimensions of length, mass and time. The dimensions of the variables are

$$[[S^{\infty}]] = [L]^{s-3}[M][T]^{-2} \tag{2a}$$

$$[r] = [L] \tag{2b}$$

$$[G] = [L]^{-1}[M][T]^{-2} \tag{2c}$$

$$[\rho] = [L]^{-3}[M] \tag{2d}$$

$$[\omega] = [T]^{-1} \tag{2e}$$

with the spatial dimension s ($= 2$ or $= 3$). The product of all these variables raised to unknown powers n_i ($i = 1, 2, \ldots, 5$) must be dimensionless,

$$[[S^{\infty}]]^{n_1}[r]^{n_2}[G]^{n_3}[\rho]^{n_4}[\omega]^{n_5} = [L]^{(s-3)n_1 + n_2 - n_3 - 3n_4}[M]^{n_1 + n_3 + n_4}[T]^{-2n_1 - 2n_3 - n_5} \tag{3}$$

This results in

$$(s-3)n_1 + n_2 - n_3 - 3n_4 = 0 \tag{4a}$$

$$n_1 + n_3 + n_4 = 0 \tag{4b}$$

$$-2n_1 - 2n_3 - n_5 = 0 \tag{4c}$$

The rank of the coefficient matrix of the system of 3 equations (equation (4)) with 5 unknowns equals 3, which permits the two unknowns n_1, n_5 to be chosen arbitrarily. For $n_1 = 1$, $n_5 = 0$, the other unknowns are $n_2 = 2 - s$, $n_3 = -1$, $n_4 = 0$, yielding the first dimensionless variable $[S^\infty]r^{2-s}G^{-1}$. For $n_1 = 0$, $n_5 = 1$, the other unknowns are $n_2 = 1$, $n_3 = -0{\cdot}5$, $n_4 = 0{\cdot}5$, resulting in the second dimensionless variable $rG^{-0{\cdot}5}\rho^{0{\cdot}5}\omega$, which is the *dimensionless frequency*

$$a_0 = \frac{\omega r}{c_s} \tag{5}$$

with the shear-wave velocity $c_s = \sqrt{G/\rho}$. The first dimensionless variable $[S^\infty]r^{2-s}G^{-1}$ will be a function $[\bar{S}^\infty]$ of the second dimensionless variable a_0 (and of ν) yielding

$$[S^\infty(r, \omega)] = Gr^{s-2}[\bar{S}^\infty(a_0)] \tag{6}$$

The arbitrary function $[\bar{S}^\infty(a_0)]$ cannot be determined based on dimensional analysis. ω and r do not appear explicitly in $[\bar{S}^\infty(a_0)]$, but only as a product in a_0 (equation (5)).

The variation of the dynamic-stiffness matrix as a function of the characteristic length r and of the excitation frequency ω is studied. $[\bar{S}^\infty(a_0)]$ is a function of one independent variable, i.e. a_0. For constant ω, $[\bar{S}^\infty(a_0)]$ is a function of r, or just as valid, for constant r, $[\bar{S}^\infty(a_0)]$ is a function or ω. The same change in a_0 can be achieved by varying the values of either r or ω with the other fixed. The derivative thus follows for a constant ω varying r as

$$[\bar{S}^\infty(a_0)]_{,a_0} = \frac{c_s}{\omega}[\bar{S}^\infty(a_0)]_{,r} \tag{7a}$$

and the same result is calculated for a constant r but varying ω as

$$[\bar{S}^\infty(a_0)]_{,a_0} = \frac{c_s}{r}[\bar{S}^\infty(a_0)]_{,\omega} \tag{7b}$$

Setting the two right-hand sides of equation (7) equal yields

$$r[\bar{S}^\infty(a_0)]_{,r} = \omega[\bar{S}^\infty(a_0)]_{,\omega} \tag{8}$$

The partial derivative of $[\bar{S}^\infty(a_0)]$ with respect to r can thus be replaced by that with respect to ω for similar interfaces. The partial derivatives with respect to r and ω are calculated from equation (6) as

$$[\bar{S}^\infty(a_0)]_{,r} = \frac{1}{Gr^{s-2}}\left(-\frac{s-2}{r}[S^\infty(r, \omega)] + [S^\infty(r, \omega)]_{,r}\right) \tag{9a}$$

$$[\bar{S}^\infty(a_0)]_{,\omega} = \frac{1}{Gr^{s-2}}[S^\infty(r, \omega)]_{,\omega} \tag{9b}$$

Substituting equation (9) into equation (8) leads to

$$r[S^\infty(r, \omega)]_{,r} = (s-2)[S^\infty(r, \omega)] + \omega[S^\infty(r, \omega)]_{,\omega} \tag{10}$$

3.2. Assemblage of finite-element cell and unbounded medium

The force–displacement relationship of the finite-element cell located between the interior and exterior boundaries (Figure 4) after partitioning is written as

$$\begin{bmatrix} [S_{ii}(\omega)] & [S_{ie}(\omega)] \\ [S_{ei}(\omega)] & [S_{ee}(\omega)] \end{bmatrix} \begin{Bmatrix} \{u_i(\omega)\} \\ \{u_e(\omega)\} \end{Bmatrix} = \begin{Bmatrix} \{P_i(\omega)\} \\ \{P_e(\omega)\} \end{Bmatrix} \tag{11}$$

with the amplitudes of the displacements $\{u(\omega)\}$ and of the nodal forces $\{P(\omega)\}$. The dynamic-stiffness matrix equals

$$[S(\omega)] = [K] - \omega^2[M] \tag{12}$$

with the static-stifness matrix $[K]$ and the mass matrix $[M]$ of the finite-element cell.

The interaction force–displacement relationship of the unbounded medium at the interfaces corresponding to the interior and exterior boundaries is formulated as

$$\{R_i(\omega)\} = [S_i^{\infty}(\omega)]\{u_i(\omega)\} \tag{13a}$$

$$\{R_e(\omega)\} = [S_e^{\infty}(\omega)]\{u_e(\omega)\} \tag{13b}$$

Note that by using the same displacement amplitudes at the interfaces (equations (11) and (13)) compatibility is enforced. Formulating equilibrium at the interior and exterior boundaries relates the interaction force amplitudes of the unbounded medium to the force amplitudes of the cell

$$\{P_i(\omega)\} = \{R_i(\omega)\} \tag{14a}$$

$$\{P_e(\omega)\} = -\{R_e(\omega)\} \tag{14b}$$

Eliminating $\{P(\omega)\}$ and $\{R(\omega)\}$ by substituting equations (11) and (13) into equation (14) leads to

$$\begin{bmatrix} [S_{ii}(\omega)] & [S_{ie}(\omega)] \\ [S_{ei}(\omega)] & [S_{ee}(\omega)] \end{bmatrix} \begin{Bmatrix} \{u_i(\omega)\} \\ \{u_e(\omega)\} \end{Bmatrix} = \begin{bmatrix} [S_i^{\infty}(\omega)] & 0 \\ 0 & -[S_e^{\infty}(\omega)] \end{bmatrix} \begin{Bmatrix} \{u_i(\omega)\} \\ \{u_e(\omega)\} \end{Bmatrix} \tag{15}$$

The relationship linking $[S_i^{\infty}(\omega)]$ and $[S_e^{\infty}(\omega)]$ can be derived by eliminating $\{u_e(\omega)\}$ from equation (15) for an arbitrary $\{u_i(\omega)\}$ resulting in

$$[S_i^{\infty}(\omega)] = [S_{ii}(\omega)] - [S_{ie}(\omega)]([S_e^{\infty}(\omega)] + [S_{ee}(\omega)])^{-1}[S_{ei}(\omega)] \tag{16}$$

3.3. Coefficient matrices of finite-element cell

In a three-dimensional unbounded medium–structure-interaction analysis the structure–medium interface is, in general, a doubly curved finite surface, which is discretized using a general two-dimensional mesh of

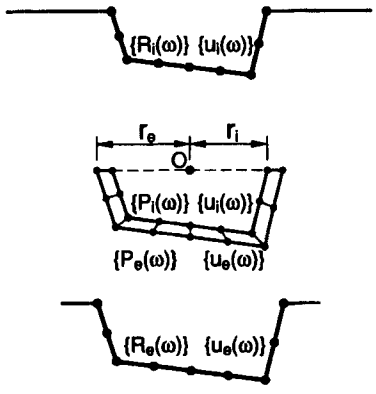

Figure 4. Finite-element region between interior and exterior boundaries and corresponding interfaces of unbounded medium

isoparametric surface finite elements (shaded area in Figure 5(a)). Starting from this mesh a three-dimensional finite-element cell satisfying similarity with a single element in the radial direction is constructed for the derivation of the consistent infinitesimal finite-element cell equation. In the radial direction of the finite element of the cell a linear shape function is introduced. To construct the static-stiffness and mass matrices of the isoparametric three-dimensional finite element, its parent element is addressed. As an example the parent element with 8 nodes on the structure–medium interface is shown in Figure 5(b). The ξ-axis of the parent element corresponds to the radial direction which points from the structure–medium interface towards infinity. At the interior boundary (which coincides with the structure–medium interface) and at the exterior boundary the values $\xi_i = -1$ and $\xi_e = +1$ result.

On the interior boundary, $\{N(\eta, \zeta)\}$ denotes the shape functions of the two-dimensional surface finite element. The corresponding 8-node quadrilateral parent element is shown in Figure 5(c). The shape functions of the three-dimensional parent element $\{\hat{N}(\xi, \eta, \zeta) = \{\hat{N}\}$ (the symbol circumflex $\hat{}$ denotes the three-dimensional finite element) are generated from those of the two-dimensional parent element $\{N(\eta, \zeta)\} = \{N\}$. It is appropriate to decompose the shape function vector $\{\hat{N}\}$ of the three-dimensional element into two subvectors corresponding to the nodes on the interior boundary i and the exterior boundary e. For the conciseness of the derivation, a subscript, e.g. j, is introduced as an index which assumes either the value of i or e. This subscript is placed outside the brace used to denote the vector. When the subscript is assigned a fixed value i or e, it is moved inside the brace. The same convention applies also to co-ordinate vectors, stiffness and mass matrices and some intermediate quantities. After this decomposition of the shape function vector with respect to the interior and exterior boundaries

$$\{\hat{N}\} = \begin{Bmatrix} \{\hat{N}_i\} \\ \{\hat{N}_e\} \end{Bmatrix} \tag{17}$$

the subvectors are equal to

$$\{\hat{N}\}_j = \tfrac{1}{2}(1 + \xi_j \xi)\{N\} \quad (j = \mathrm{i}, \mathrm{e}) \tag{18}$$

with a typical element

$$\hat{N}_{jk} = \tfrac{1}{2}(1 + \xi_j \xi) N_k \quad (j = \mathrm{i}, \mathrm{e}; \quad k = 1, 2, \ldots) \tag{19}$$

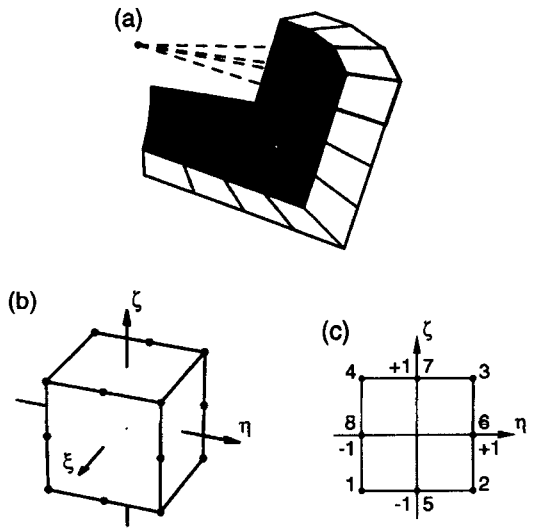

Figure 5. (a) Structure–medium interface with adjacent three-dimensional finite-element cell. (b) Three-dimensional parent element of finite element of cell. (c) Two-dimensional parent element of finite element on discretized structure–medium interface

j denotes the interior or exterior boundary and k the node number of the two-dimensional parent element. Due to similarity, the co-ordinates of the nodes on the exterior boundary $\{x_e\}, \{y_e\}, \{z_e\}$ can be expressed by those of the nodes on the interior boundary $\{x\}, \{y\}, \{z\}$ and the dimensionless cell width w as (equation (1))

$$\{x_e\} = (1 + w)\{x\} \tag{20a}$$

$$\{y_e\} = (1 + w)\{y\} \tag{20b}$$

$$\{z_e\} = (1 + w)\{z\} \tag{20c}$$

Note that the subscript i for the co-ordinates of the interior boundary, the structure–medium interface, is omitted (as in an actual application only the latter is discretized). The nodal co-ordinates of the three-dimensional finite element $\{\hat{x}\}, \{\hat{y}\}, \{\hat{z}\}$ are constructed by assembling those of the nodes on the interior and exterior boundaries $\{x\}$ and $\{x_e\}$, $\{y\}$ and $\{y_e\}$, $\{z\}$ and $\{z_e\}$.

Introducing the isoparametric mapping rule and with equations (17), (18) and (20)

$$\hat{x} = \{\hat{N}\}^T\{\hat{x}\} = \{\hat{N}_i\}^T\{x\} + \{\hat{N}_e\}^T\{x_e\} = \left(1 + \frac{w}{2}(1 + \xi)\right)\{N\}^T\{x\} \tag{21a}$$

$$\hat{y} = \left(1 + \frac{w}{2}(1 + \xi)\right)\{N\}^T\{y\} \tag{21b}$$

$$\hat{z} = \left(1 + \frac{w}{2}(1 + \xi)\right)\{N\}^T\{z\} \tag{21c}$$

follow. The Jacobian matrix of the three-dimensional finite element equals

$$[\hat{J}] = \begin{bmatrix} \hat{x}_{,\xi} & \hat{y}_{,\xi} & \hat{z}_{,\xi} \\ \hat{x}_{,\eta} & \hat{y}_{,\eta} & \hat{z}_{,\eta} \\ \hat{x}_{,\zeta} & \hat{y}_{,\zeta} & \hat{z}_{,\zeta} \end{bmatrix} = \begin{bmatrix} \frac{w}{2} & & \\ & 1 + \frac{w}{2}(1 + \xi) & \\ & & 1 + \frac{w}{2}(1 + \xi) \end{bmatrix} [J] \tag{22}$$

where the abbreviation

$$[J] = \begin{bmatrix} \{N\}^T\{x\} & \{N\}^T\{y\} & \{N\}^T\{z\} \\ \{N_{,\eta}\}^T\{x\} & \{N_{,\eta}\}^T\{y\} & \{N_{,\eta}\}^T\{z\} \\ \{N_{,\zeta}\}^T\{x\} & \{N_{,\zeta}\}^T\{y\} & \{N_{,\zeta}\}^T\{z\} \end{bmatrix} \tag{23}$$

is introduced. The determinant of the Jacobian matrix equals

$$|\hat{J}| = \frac{w}{2}\left(1 + \frac{w}{2}(1 + \xi)\right)^2 |J| \tag{24}$$

The inverse of the Jacobian matrix follows as

$$[\hat{J}]^{-1} = [J]^{-1} \begin{bmatrix} \frac{2}{w} & & \\ & \frac{2}{2 + w(1 + \xi)} & \\ & & \frac{2}{2 + w(1 + \xi)} \end{bmatrix} \tag{25}$$

where $[J]^{-1}$ is denoted as

$$[J]^{-1} = \begin{bmatrix} j_{11} & j_{12} & j_{13} \\ j_{21} & j_{22} & j_{23} \\ j_{31} & j_{32} & j_{33} \end{bmatrix} \tag{26}$$

The derivatives of the shape functions are formulated as

$$\begin{Bmatrix} \hat{N}_{jk,\hat{x}} \\ \hat{N}_{jk,\hat{y}} \\ \hat{N}_{jk,\hat{z}} \end{Bmatrix} = [\hat{J}]^{-1} \begin{Bmatrix} \hat{N}_{jk,\xi} \\ \hat{N}_{jk,\eta} \\ \hat{N}_{jk,\zeta} \end{Bmatrix}$$

$$= \frac{\xi_j}{w} \begin{Bmatrix} j_{11} \\ j_{21} \\ j_{31} \end{Bmatrix} N_k + \frac{1 + \xi_j \xi}{2 + w(1 + \xi)} \left(\begin{Bmatrix} j_{21} \\ j_{22} \\ j_{23} \end{Bmatrix} N_{k,\eta} + \begin{Bmatrix} j_{13} \\ j_{23} \\ j_{33} \end{Bmatrix} N_{k,\zeta} \right) \tag{27}$$

The strain-nodal displacement matrix with the strain vector arranged as $[\varepsilon_x \ \varepsilon_y \ \varepsilon_z \ \gamma_{yz} \ \gamma_{xz} \ \gamma_{xy}]^T$ equals

$$[B]_{jk} = \begin{bmatrix} \hat{N}_{jk,\hat{x}} & 0 & 0 \\ 0 & \hat{N}_{jk,\hat{y}} & 0 \\ 0 & 0 & \hat{N}_{jk,\hat{z}} \\ 0 & \hat{N}_{jk,\hat{z}} & \hat{N}_{jk,\hat{y}} \\ \hat{N}_{jk,\hat{z}} & 0 & \hat{N}_{jk,\hat{x}} \\ \hat{N}_{jk,\hat{y}} & \hat{N}_{jk,\hat{x}} & 0 \end{bmatrix} = \frac{\xi_j}{w} [B^1]_k + \frac{1 + \xi_j \xi}{2 + w(1 + \xi)} [B^2]_k \tag{28}$$

where

$$[B^1]_k = \begin{bmatrix} j_{11} & 0 & 0 \\ 0 & j_{21} & 0 \\ 0 & 0 & j_{31} \\ 0 & j_{31} & j_{21} \\ j_{31} & 0 & j_{11} \\ j_{21} & j_{11} & 0 \end{bmatrix} N_k \tag{29a}$$

$$[B^2]_k = \begin{bmatrix} j_{12} & 0 & 0 \\ 0 & j_{22} & 0 \\ 0 & 0 & j_{32} \\ 0 & j_{32} & j_{22} \\ j_{32} & 0 & j_{12} \\ j_{22} & j_{12} & 0 \end{bmatrix} N_{k,\eta} + \begin{bmatrix} j_{13} & 0 & 0 \\ 0 & j_{23} & 0 \\ 0 & 0 & j_{33} \\ 0 & j_{33} & j_{23} \\ j_{33} & 0 & j_{13} \\ j_{23} & j_{13} & 0 \end{bmatrix} N_{k,\zeta} \tag{29b}$$

Assembling $[B^1]_k$ and $[B^2]_k$ of all nodes yields $[B^1]$ and $[B^2]$, which are not a function of ξ. $[B]$ is decomposed with respect to the interior and exterior boundaries as

$$[B] = [[B_i] \quad [B_e]] \tag{30}$$

with

$$[B]_j = \frac{\xi_j}{w}[B^1] + \frac{1 + \xi_j \xi}{2 + w(1 + \xi)}[B^2] \quad (j = \mathrm{i}, \mathrm{e}) \tag{31}$$

The static-stiffness matrix of the three-dimensional finite element equals

$$[K] = \int_V [B]^T [D][B] \, \mathrm{d}V \tag{32}$$

with the integration over the volume V of the element. $[D]$ is the three-dimensional (in general, anisotropic) elasticity matrix of the stress–strain relationship and is positive definite. $[K]$ is decomposed into submatrices with respect to the interior and exterior boundaries as (j = i, e; l = i, e)

$$[K]_{jl} = \int_V [B]_j^T [D][B]_l \, \mathrm{d}V = \int_{-1}^{+1} \int_{-1}^{+1} \int_{-1}^{+1} [B]_j^T [D][B]_l |\hat{J}| \, \mathrm{d}\xi \, \mathrm{d}\eta \, \mathrm{d}\zeta \tag{33}$$

Substituting equations (31) and (24) into equation (33) yields a polynomial in ξ which can be integrated analytically. Decomposition with respect to the dimensionless cell width w for later use in the consistent infinitesimal finite-element cell equation yields without introducing any approximation

$$[K]_{jl} = \frac{1}{w}[K^0]_{jl} + [K^1]_{jl} + w[K^2]_{jl} \tag{34}$$

where

$$[K^0]_{jl} = \xi_j \xi_l [E^0] \tag{35a}$$

$$[K^1]_{jl} = \xi_j \xi_l [E^0] + \frac{\xi_l}{2}[E^1] + \frac{\xi_j}{2}[E^1]^T \tag{35b}$$

$$[K^2]_{jl} = \frac{\xi_j \xi_l}{3}[E^0] + \left(\frac{\xi_l}{4} + \frac{\xi_j \xi_l}{12}\right)[E^1] + \left(\frac{\xi_j}{4} + \frac{\xi_j \xi_l}{12}\right)[E^1]^T + \left(\frac{1}{4} + \frac{\xi_j \xi_l}{12}\right)[E^2] \tag{35c}$$

with

$$[E^0] = \int_{-1}^{+1} \int_{-1}^{+1} [B^1]^T [D][B^1] |J| \, \mathrm{d}\eta \, \mathrm{d}\zeta \tag{36a}$$

$$[E^1] = \int_{-1}^{+1} \int_{-1}^{+1} [B^2]^T [D][B^1] |J| \, \mathrm{d}\eta \, \mathrm{d}\zeta \tag{36b}$$

$$[E^2] = \int_{-1}^{+1} \int_{-1}^{+1} [B^2]^T [D][B^2] |J| \, \mathrm{d}\eta \, \mathrm{d}\zeta \tag{36c}$$

The coefficient matrices specified in equation (36) are determined by numerical integration. Note that $[E^0]$, $[E^1]$ and $[E^2]$ depend on the discretization of the structure–medium interface and not on that in the radial direction. $[E^0]$ is positive definite, and $[E^2]$ is semi-positive definite (and symmetric).

The mass matrix with the mass density ρ equals

$$[M] = \int_V \rho[\hat{N}]^T[\hat{N}]\,dV \tag{37}$$

Its submatrices are decomposed with respect to the interior and exterior boundaries as (j = i, e; l = i, e)

$$[M]_{jl} = \int_V \rho[\hat{N}]_j^T[\hat{N}]_l\,dV = \int_{-1}^{+1}\int_{-1}^{+1}\int_{-1}^{+1} \rho[\hat{N}]_j^T[\hat{N}]_l|\hat{J}|\,d\xi\,d\eta\,d\zeta \tag{38}$$

where

$$[\hat{N}]_j = \tfrac{1}{2}(1 + \xi_j\xi)[N] \quad (j = \text{i, e}) \tag{39}$$

with

$$[N] = \begin{bmatrix} N_1 & & N_2 & & \cdots \\ & N_1 & & N_2 & \cdots \\ & & N_1 & & N_2 \quad \cdots \end{bmatrix} \tag{40}$$

Equation (24) is substituted into equation (38). Again the integration in the ξ-direction is performed analytically. As will become apparent, the terms of order in w higher than 1 can be neglected when the limit $w \to 0$ is performed analytically. Thus,

$$[M]_{jl} = w[M^2]_{jl} + O(w^2) = \frac{w}{4}\left(1 + \frac{\xi_j\xi_l}{3}\right)[M^0] + O(w^2) \tag{41}$$

applies with the coefficient matrix

$$[M^0] = \int_{-1}^{+1}\int_{-1}^{+1} \rho[N]^T[N]|J|\,d\eta\,d\zeta \tag{42}$$

Note that $[M^0]$ is positive definite.

To derive the consistent infinitesimal finite-element cell equation, the following relationships will be used:

$$[K_{ii}^0] = -[K_{ie}^0] = -[K_{ei}^0] = [K_{ee}^0] = [E^0] \tag{43a}$$

$$[K_{ie}^1] + [K_{ee}^1] = -([K_{ii}^1] + [K_{ie}^1])^T = [E^1] \tag{43b}$$

$$[K_{ii}^2] + [K_{ie}^2] + [K_{ei}^2] + [K_{ee}^2] = [E^2] \tag{43c}$$

$$[M_{ii}^2] + [M_{ie}^2] + [M_{ei}^2] + [M_{ee}^2] = [M^0] \tag{44}$$

Equation (43) follows from equation (35) with $\xi_i = -1$, $\xi_e = +1$ and equation (44) from equation (41). The right-hand sides of equations (43) and (44) are defined in equations (36) and (42), respectively. $[E^0]$, $[E^1]$, $[E^2]$ and $[M^0]$ are the coefficient matrices of one surface finite element.

As for the static-stiffness and mass matrices the coefficient matrices $[E^0]$, $[E^1]$, $[E^2]$ and $[M^0]$ are assembled to form those of the structure–medium interface. The latter will thus be banded. To simplify the nomenclature, the same symbols are used for the assembled coefficient, static-stiffness and mass matrices in the following. For the assembled static-stiffness and mass matrices, equations (43) and (44) still hold.

The coefficient matrices of the finite-element cell for the two-dimensional equation follow straightforwardly from the three-dimensional case. All terms in z and ζ are deleted. The definition of $[E^0]$, $[E^1]$ and $[E^2]$ in

equation (36) and of $[M^0]$ in equation (42) still apply (deleting the integration in the ζ-direction) with

$$[B^1]_k = \begin{bmatrix} j_{11} & 0 \\ 0 & j_{21} \\ j_{21} & j_{11} \end{bmatrix} N_k \tag{45a}$$

$$[B^2]_k = \begin{bmatrix} j_{12} & 0 \\ 0 & j_{22} \\ j_{22} & j_{12} \end{bmatrix} N_{k,\eta} \tag{45b}$$

$$[N] = \begin{bmatrix} N_1 & & N_2 & & \cdots \\ & N_1 & & N_2 & \cdots \end{bmatrix} \tag{46}$$

3.4. Consistent infinitesimal finite-element cell equation in frequency domain

The consistent infinitesimal finite-element cell equation is derived using the relationship of the dynamic-stiffness matrices based on similarity formulated in the continuous form (equation (10)) and the relationship based on assemblage (equation (16)), for which the limit of infinitesimal cell width must be performed.

Equation (16) is reformulated as

$$([S_e^\infty(\omega)] + [S_{ee}(\omega)])[S_{ie}(\omega)]^{-1}([S_i^\infty(\omega)] - [S_{ii}(\omega)]) + [S_{ei}(\omega)] = 0 \tag{47}$$

The dynamic-stiffness submatrices of the cell are written as follows. For instance,

$$[S_{ii}(\omega)] = [K_{ii}] - \omega^2[M_{ii}] \tag{48}$$

applies with $[K_{ii}]$ specified in equation (34) and $[M_{ii}]$ in equation (41). This yields

$$[S_{ii}(\omega)] = \frac{1}{w}[K_{ii}^0] + [K_{ii}^1] + w[K_{ii}^2] - w\omega^2[M_{ii}^2] + O(w^2) \tag{49}$$

Using equation (43a) leads to

$$[S_{ii}(\omega)] = \frac{1}{w}[E^0] + [K_{ii}^1] + w([K_{ii}^2] - \omega^2[M_{ii}^2]) + O(w^2) \tag{50a}$$

Analogously,

$$[S_{ie}(\omega)] = -\frac{1}{w}[E^0] + [K_{ie}^1] + w([K_{ie}^2] - \omega^2[M_{ie}^2]) + O(w^2) \tag{50b}$$

$$[S_{ei}(\omega)] = -\frac{1}{w}[E^0] + [K_{ei}^1] + w([K_{ei}^2] - \omega^2[M_{ei}^2]) + O(w^2) \tag{50c}$$

$$[S_{ee}(\omega)] = \frac{1}{w}[E^0] + [K_{ee}^1] + w([K_{ee}^2] - \omega^2[M_{ee}^2]) + O(w^2) \tag{50d}$$

follow. The inverse $[S_{ie}(\omega)]^{-1}$ appearing in equation (47) is expressed as a polynomial in w with the unknown coefficient matrices $[A]$ and $[B]$,

$$[S_{ie}(\omega)]^{-1} = -w[E^0]^{-1} + w^2[A] + w^3[B] + O(w^4) \tag{51}$$

The coefficient matrix of w is equal to the inverse of that of $1/w$ in equation (50b). $[A]$ and $[B]$ follow from

$$[I] = [S_{ie}][S_{ie}]^{-1} = [I] - w([K^1_{ie}][E^0]^{-1} + [E^0][A]) - w^2(([K^2_{ie}] - \omega^2[M^2_{ie}])[E_0]^{-1} - [K^1_{ie}][A] + [E^0][B]) + O(w^3) \tag{52}$$

Setting the coefficient matrices of w and w^2 equal to zero yields

$$[A] = -[E^0]^{-1}[K^1_{ie}][E^0]^{-1} \tag{53a}$$

$$[B] = -[E^0]^{-1}([K^1_{ie}][E^0]^{-1}[K^1_{ie}] - ([K^2_{ie}] - \omega^2[M^2_{ie}]))[E^0]^{-1} \tag{53b}$$

Substituting equations (50) and (51) with equation (53) into equation (47) leads to

$$\underbrace{[K^1_{ii}] + [K^1_{ie}] + [K^1_{ei}] + [K^1_{ee}]}_{1} - w\underbrace{([S^\infty_e(\omega)] + [K^1_{ie}] + [K^1_{ee}])[E^0]^{-1}([S^\infty_i(\omega)] - [K^1_{ii}] - [K^1_{ie}])}_{2} + \underbrace{[S^\infty_e(\omega)] - [S^\infty_i(\omega)]}_{3} + w\underbrace{([K^2_{ii}] + [K^2_{ie}] + [K^2_{ei}] + [K^2_{ee}]}_{4} - \omega^2\underbrace{([M^2_{ii}] + [M^2_{ie}] + [M^2_{ei}] + [M^2_{ee}])}_{5} = O(w^2) \tag{54}$$

The sum identified by 1 in equation (54) vanishes according to equation (43b). Equation (43b) is substituted in the term identified by 2. The sums identified by 4 and 5 are transformed using equations (43c) and (44), respectively. Dividing equation (54) by w results in

$$([S^\infty_e(\omega)] + [E^1])[E^0]^{-1}([S^\infty_i(\omega)] + [E^1]^T) - \frac{[S^\infty_e(\omega)] - [S^\infty_i(\omega)]}{w} - [E^2] + \omega^2[M^0] = O(w) \tag{55}$$

The limit of $w \to 0$ can now be performed. With w defined in equation (1)

$$\lim_{w\to 0} \frac{[S^\infty_e(\omega)] - [S^\infty_i(\omega)]}{w} = \lim_{r_e \to r_i} r_i \frac{[S^\infty_e(\omega)] - [S^\infty_i(\omega)]}{r_e - r_i} = r[S^\infty(\omega)]_{,r} \tag{56}$$

results with $[S^\infty(\omega)] = [S^\infty_i(\omega)]$ and $r = r_i$. With $[S^\infty_e(\omega)] = [S^\infty_i(\omega)] + O(w)$, the limit of equation (55) equals

$$([S^\infty(\omega)] + [E^1])[E^0]^{-1}([S^\infty(\omega)] + [E^1]^T) - r[S^\infty(\omega)]_{,r} - [E^2] + \omega^2[M^0] = O(w) \tag{57}$$

Substituting $r[S^\infty(\omega)]_{,r}$ of equation (10) based on similarity in equation (57) leads to

$$([S^\infty(\omega)] + [E^1])[E^0]^{-1}([S^\infty(\omega)] + [E^1]^T) - (s-2)[S^\infty(\omega)] - \omega[S^\infty(\omega)]_{,\omega} - [E^2] + \omega^2[M^0] = 0 \tag{58}$$

In an actual application a specific structure–medium interface is addressed which fixes r. The dynamic-stiffness matrix thus becomes a function of ω only. The partial derivative $[S^\infty(r, \omega)]_{,\omega}$ in equation (10) is replaced by $[S^\infty(\omega)]_{,\omega}$.

This represnts the *consistent infinitesimal finite-element cell equation formulated in the frequency domain.* It is a system of non-linear ordinary differential equations of first order in the independent variable which is the frequency ω. If $[S^\infty(\omega)]$ is known at a specific frequency, starting from this boundary condition $[S^\infty(\omega)]$ can be calculated for increasing and decreasing frequencies by integrating equation (58) numerically. The integration of ordinary differential equations is well known and will not be repeated here. Powerful algorithms are e.g. listed in Reference 4.

The boundary condition must satisfy the radiation condition in the frequency domain. Obviously, the static-stiffness matrix cannot be used. The radiation condition is formulated at an infinite distance from the structure–medium interface which corresponds to an infinite characteristic length r. The associated dimensionless frequency $a_0 = \omega r/c_s$ is thus infinite, which can also be achieved by an infinite ω. The boundary condition $[S^\infty(\omega)]$ satisfying the radiation condition is formulated at infinite ω. In an actual calculation, a large ω is selected. Thus, the high-frequency behaviour of $[S^\infty(\omega)]$ is studied examining the asymptotic expansion of equation (58).

4. ASYMPTOTIC EXPANSION FOR HIGH FREQUENCY

The dynamic-stiffness matrix $[S^\infty(\omega)]$ at high frequency is expanded in a power series of $i\omega$ in descending order starting at one

$$[S^\infty(\omega)] \approx i\omega[C_\infty] + [K_\infty] + \sum_{j=1}^{m} \frac{1}{(i\omega)^j}[A_j] \tag{59}$$

The first two terms on the right-hand side represent the singular part $[S_s^\infty(\omega)]$ with the constant dashpot matrix $[C_\infty]$ and the constant spring matrix $[K_\infty]$ (Reference 5, p. 256). The third term denotes the asymptotic expansion with m terms of the regular part $[S_r^\infty(\omega)]$ with the unknown coefficient matrices $[A_j]$ $(j = 1, \ldots, m)$. A concise formulation results when the transformation based on the following eigenvalue problem is introduced:

$$[M^0][\Phi] = [E^0][\Phi]\lceil \Lambda^2 \rfloor \tag{60}$$

$[M^0]$ and $[E^0]$ are positive-definite matrices resulting in positive eigenvalues $\lceil \Lambda^2 \rfloor$. The eigenvectors $[\Phi]$ are normalized as

$$[\Phi]^T[E^0][\Phi] = [I] \tag{61}$$

yielding

$$[\Phi]^T[M^0][\Phi] = \lceil \Lambda^2 \rfloor \tag{62}$$

and

$$[E^0]^{-1} = [\Phi][\Phi]^T \tag{63}$$

Premultiplying equation (58) by $[\Phi]^T$ and postmultiplying by $[\Phi]$ results in

$$([s^\infty(\omega)] + [e^1])([s^\infty(\omega)] + [e^1]^T) - (s-2)[s^\infty(\omega)] - \omega[s^\infty(\omega)]_{,\omega} - [e^2] + \omega^2\lceil \Lambda^2 \rfloor = 0 \tag{64}$$

where

$$[s^\infty(\omega)] = [\Phi]^T[S^\infty(\omega)][\Phi] \tag{65}$$

and

$$[e^1] = [\Phi]^T[E^1][\Phi] \tag{66a}$$

$$[e^2] = [\Phi]^T[E^2][\Phi] \tag{66b}$$

Substituting equation (59) into equation (65) yields

$$[s^\infty(\omega)] \approx i\omega[c_\infty] + [k_\infty] + \sum_{j=1}^{m} \frac{1}{(i\omega)^j}[a_j] \tag{67}$$

with

$$[c_\infty] = [\Phi]^T[C_\infty][\Phi] \tag{68a}$$

$$[k_\infty] = [\Phi]^T[K_\infty][\Phi] \tag{68b}$$

$$[a_j] = [\Phi]^T[A_j][\Phi] \tag{68c}$$

Substituting equation (67) into equation (64) and rearranging in descending order of the power series of $i\omega$ leads to

$$\begin{aligned}(i\omega)^2([c_\infty]^2 - \lceil \Lambda^2 \rfloor) + i\omega([c_\infty][k_\infty] + [k_\infty][c_\infty] + [c_\infty][e^1]^T + [e^1][c_\infty] - (s-1)[c_\infty]) \\ + [c_\infty][a_1] + [a_1][c_\infty] + ([k_\infty] + [e^1])([k_\infty] + [e^1]^T) - (s-2)[k_\infty] - [e^2] \\ + \frac{1}{i\omega}([c_\infty][a_2] + [a_2][c_\infty] + ([k_\infty] + [e^1])[a_1] + [a_1]([k_\infty] + [e^1]^T) - (s-3)[a_1]) \approx 0\end{aligned} \tag{69}$$

In equation (69), $m = 2$ is selected. The generalization to any m leading to additional terms is straightforward.

The coefficient matrix of each term of the power series in $i\omega$ is set equal to zero in descending order. The first yields

$$[c_\infty]^2 = \lceil \Lambda^2 \rfloor \tag{70}$$

Selecting the positive roots of each element on the diagonal of $\lceil \Lambda^2 \rfloor$ leads to

$$[c_\infty] = \lceil \Lambda \rfloor \tag{71}$$

The dashpot matrix $[C_\infty]$ follows from equation (68a) as

$$[C_\infty] = ([\Phi]^{-1})^T \lceil \Lambda \rfloor [\Phi]^{-1} \tag{72}$$

As each coefficient of $\lceil \Lambda \rfloor$ is positive, $[C_\infty]$ will be positive definite.

The second term in equation (69) results after substituting equation (71) in

$$\lceil \Lambda \rfloor [k_\infty] + [k_\infty] \lceil \Lambda \rfloor = -\lceil \Lambda \rfloor [e^1]^T - [e^1] \lceil \Lambda \rfloor + (s-1) \lceil \Lambda \rfloor \tag{73}$$

This linear equation for $[k_\infty]$ is a Lyapunov equation with a diagonal coefficient matrix $\lceil \Lambda \rfloor$. Its solution for each element $k_{\infty kl}$ equals

$$k_{\infty kl} = \frac{1}{\Lambda_k + \Lambda_l}(-\Lambda_k e^1_{lk} - \Lambda_l e^1_{kl} + (s-1)\Lambda_k \delta_{kl}) \tag{74}$$

with the Kronecker delta δ_{kl} ($= 1$ for $k = l$; $= 0$ for $k \neq l$). The spring matrix $[K_\infty]$ is calculated from equation (68b) as

$$[K_\infty] = ([\Phi]^{-1})^T [k_\infty] [\Phi]^{-1} \tag{75}$$

The third term in equation (69) leads after substituting equation (71) with the known $[k_\infty]$ to

$$\lceil \Lambda \rfloor [a_1] + [a_1] \lceil \Lambda \rfloor = -([k_\infty] + [e^1])([k_\infty] + [e^1]^T) + (s-2)[k_\infty] + [e^2] \tag{76}$$

This equation for $[a_1]$ is in the same form as equation (73). Analogously, $[a_2]$ is determined from the fourth term in equation (69) with the known $[c_\infty] = \lceil \Lambda \rfloor$, $[k_\infty]$ and $[a_1]$,

$$\lceil \Lambda \rfloor [a_2] + [a_2] \lceil \Lambda \rfloor = -([k_\infty] + [e^1])[a_1] - [a_1]([k_\infty] + [e^1]^T) + (s-3)[a_1] \tag{77}$$

The coefficient matrices $[A_j]$ result from equation (68c) as

$$[A_j] = ([\Phi]^{-1})^T [a_j] [\Phi]^{-1} \tag{78}$$

After calculating $[C_\infty]$, $[K_\infty]$, $[A_1]$ and $[A_2]$, the asymptotic behaviour for $m = 2$ follows from equation (59).

In an actual application of the consistent infinitesimal finite-element cell method in the frequency domain the boundary condition at the specified high frequency ω_h, which replaces $\omega \to \infty$, $[S^\infty(\omega_h)]$ follows from equation (59) for a selected m. The dashpot matrix $[C_\infty]$ is calculated after solving an eigenvalue problem (equation (72)), and the spring matrix $[K_\infty]$ (equation (75)) as well as the coefficient matrices of the asymptotic expansion $[A_j]$ (equation (78)) follow from Lyapunov equations. $[S^\infty(\omega_h)]$ is then used as the starting value to integrate the consistent infinitesimal finite-element cell equation (equation (58)) for decreasing ω.

5. EXAMPLES

5.1. Spherical cavity embedded in full space

The spherical cavity of radius r_0 embedded in a full space with shear modulus G, Poisson's ratio ν and mass density ρ is addressed. A uniform normal displacement amplitude $u_0(\omega)$ is prescribed on its wall, the structure–medium interface, yielding the pressure amplitude $p(\omega)$. This one-dimensional problem is solved in Section 2.3 of Reference 5. The analytical solution of the dynamic-stiffness coefficient relating $u_0(\omega)$ to the amplitude of the total interaction force $R(\omega) = 4\pi r_0^2 p(\omega)$ is specified as

$$S^\infty(\omega) = 16\pi G r_0 \left(1 + \frac{1-\nu}{2(1-2\nu)} \frac{1}{c_p} \frac{(i\omega r_0)^2}{c_p + i\omega r_0}\right) \tag{79}$$

with the dilatational-wave velocity c_p.

The coefficients E^0, E^1, E^2 and M^0 follow as

$$E^0 = 8\pi \frac{1-\nu}{1-2\nu} G r_0 \tag{80a}$$

$$E^1 = 16\pi \frac{\nu}{1-2\nu} G r_0 \tag{80b}$$

$$E^2 = 16\pi \frac{1}{1-2\nu} G r_0 \tag{80c}$$

$$M^0 = 4\pi \rho r_0^3 \tag{81}$$

Substituting equations (80) and (81) into equation (58) yields

$$\frac{1}{8\pi} \frac{1-2\nu}{1-\nu} \frac{1}{G r_0} (S^\infty(\omega))^2 - \frac{1-5\nu}{1-\nu} S^\infty(\omega) - \omega S^\infty(\omega)_{,\omega} + 4\pi r_0^3 \rho \omega^2 - 16\pi \frac{1+\nu}{1-\nu} G r_0 = 0 \tag{82}$$

The accuracy of the consistent infinitesimal finite-element cell method is investigated. First, the asymptotic expansion for high frequency, which provides the boundary condition, is examined. An asymptotic expansion can be derived from the analytical solution and used in a comparison with that of the consistent infinitesimal finite-element cell equation. The coefficients of the asymptotic expansion of the analytical solution of $S^\infty(\omega)$ specified in equation (79) for high frequency are

$$C_\infty = 4\pi r_0^2 \rho c_p \tag{83a}$$

$$K_\infty = 8\pi \frac{1-3\nu}{1-2\nu} G r_0 \tag{83b}$$

$$A_1 = 4\pi \rho c_p^3 \tag{83c}$$

$$A_2 = -4\pi \rho c_p^4 \frac{1}{r_0} \tag{83d}$$

The coefficients of the asymptotic expansion are calculated from the consistent infinitesimal finite-element cell equation. From equations (60) and (61)

$$\Lambda^2 = \frac{M^0}{E^0} \tag{84}$$

$$\Phi = (E^0)^{-0.5} \tag{85}$$

result. The dashpot coefficient C_∞ follows from equation (72) as

$$C_\infty = \frac{\Lambda}{\Phi^2} = 4\pi r_0^2 \rho c_p \tag{86}$$

and the spring coefficient K_∞ from equations (73) and (75) as

$$K_\infty = E^0 - E^1 = 8\pi \frac{1-3\nu}{1-2\nu} G r_0 \tag{87}$$

The coefficients A_1 and A_2 result from equations (76)–(78) as

$$A_1 = 4\pi \rho c_p^3 \tag{88a}$$

$$A_2 = -4\pi \rho c_p^4 \frac{1}{r_0} \tag{88b}$$

As expected, the coefficients of the asymptotic expansion C_∞, K_∞, A_1, A_2 determined from the consistent infinitesimal finite-element cell equation are identical to those of the analytical solution (equation (83)).

The consistent infinitesimal finite-element cell equation (equation (82)) is solved starting from the boundary condition evaluated at different frequencies ω_h:

$$S^\infty(\omega_h) \approx i\omega_h C_\infty + K_\infty + \sum_{j=1}^{m} \frac{1}{(i\omega_h)^j} A_j \tag{89}$$

The analysis is performed for Poisson's ratio $\nu = 0{\cdot}25$ using the Bulirsch–Stoer method described in Reference 4, starting at $\omega_h = a_{0h} c_p / r_0$ for $a_{0h} = 3$ and $= 6$. The dynamic-stiffness coefficient is decomposed in the dimensionless spring coefficient $k(a_0)$ and damping coefficient $c(a_0)$ as

$$S^\infty(a_0) = K^\infty(k(a_0) + i a_0 c(a_0)) \tag{90}$$

with the static-stiffness coefficient K^∞ and the dimensionless frequency $a_0 = \omega r_0 / c_p$. As shown in Figure 6, the (small) error of the boundary condition decreases for decreasing a_0. Even for $a_{0h} = 3$ with the boundary condition $K^\infty(0{\cdot}333 + i2)$ (the analytical solution equals $K^\infty(0{\cdot}325 + i2{\cdot}025)$), the results are highly accurate.

5.2. Circular cavity embedded in full-plane

As a two-dimensional in-plane wave propagation problem with an analytical solution available, the circular cavity embedded in a full-plane is discussed (Figure 7). On its rigid wall, the structure–medium interface, a constant horizontal displacement u_0 is enforced. The radius of the cavity is r_0, and the material properties of the full-plane are chosen as the Lamé parameters λ and G, the shear modulus ($\lambda = 2G\nu/(1-2\nu)$ with Poisson's ratio ν). The shear- and dilatational-wave velocities equal

$$c_s = \sqrt{\frac{G}{\rho}} \tag{91a}$$

$$c_p = \sqrt{\frac{\lambda + 2G}{\rho}} = \sqrt{\frac{2(1-\nu)}{1-2\nu}}\, c_s \tag{91b}$$

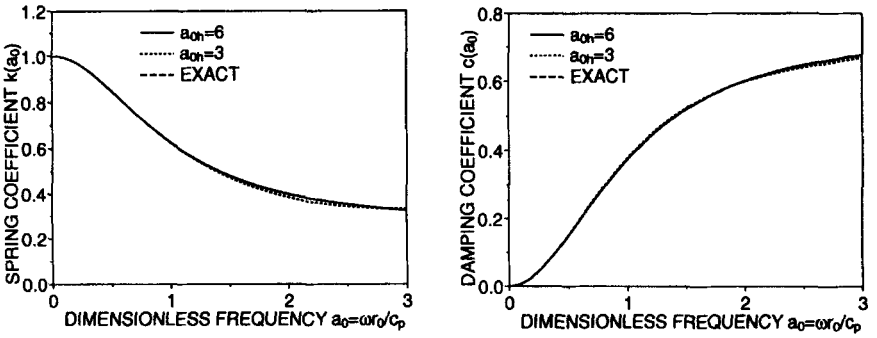

Figure 6. Dynamic-stiffness coefficient of spherical cavity for different starting values

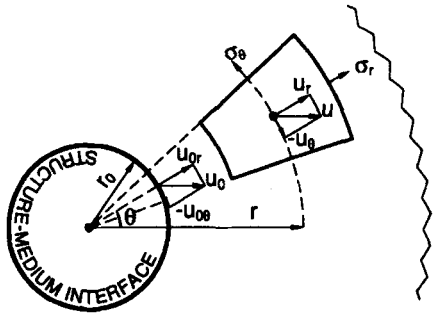

Figure 7. Circular cavity embedded in full-plane with prescribed translational motion

The analytical solution for the dynamic-stiffness coefficient equals[6]

$$S^{\infty}(a_0) = \pi G a_0^2 \frac{\alpha + \beta - 4}{\alpha\beta - \alpha - \beta} \tag{92}$$

with

$$\alpha = a_0 \frac{H_0^{(2)}(a_0)}{H_1^{(2)}(a_0)} \tag{93a}$$

$$\beta = \frac{c_s}{c_p} a_0 \frac{H_0^{(2)}\left(\frac{c_s}{c_p} a_0\right)}{H_1^{(2)}\left(\frac{c_s}{c_p} a_0\right)} \tag{93b}$$

$$a_0 = \frac{\omega r_0}{c_s} \tag{94}$$

Due to symmetry only one quarter of the structure–medium interface is discretized with 4 3-node line elements of equal length. The boundary condition of the dynamic-stiffness matrix $[S^{\infty}(\omega_h)]$ is determined from the asymptotic expansion with $m = 2$ (equation (59)) at $\omega_h = a_{0h} c_s / r_0$ for $a_{0h} = 6$. $[S^{\infty}(\omega)]$ of order 16×16 is calculated for decreasing ω with the consistent infinitesimal finite-element cell method based on the Bulirsch–Stoer method of Reference 4. The dynamic-stiffness coefficient $S^{\infty}(\omega)$ follows from

$$S^{\infty}(\omega) = \{\phi\}^{\mathrm{T}} [S^{\infty}(\omega)] \{\phi\} \tag{95}$$

with the vector $\{\phi\}$ determined from the translational motion of the rigid structure–medium interface. $S^{\infty}(\omega)$ non-dimensionalized with the shear modulus G is decomposed in $k(a_0)$ and $c(a_0)$. Excellent agreement with the analytical solution for $\nu = \frac{1}{3}$ of equation (92) results (Figure 8).

5.3. *Prism embedded in half-space*

The three-dimensional motion of a square prism of length $2b$ embedded with depth e in a half-space of shear modulus G, Poisson's ratio ν and mass density ρ (Figure 9) is calculated. The embedment ratio $e/b = \frac{2}{3}$ and $\nu = \frac{1}{3}$ are selected. The finite-element discretization of one quarter of the structure–medium interface is shown in Figure 10. The dynamic-stiffness matrix $[S^{\infty}(\omega)]$ is calculated for decreasing ω using the consistent infinitesimal finite-element cell method based on the Bulirsch–Stoer method of Reference 4, starting from the

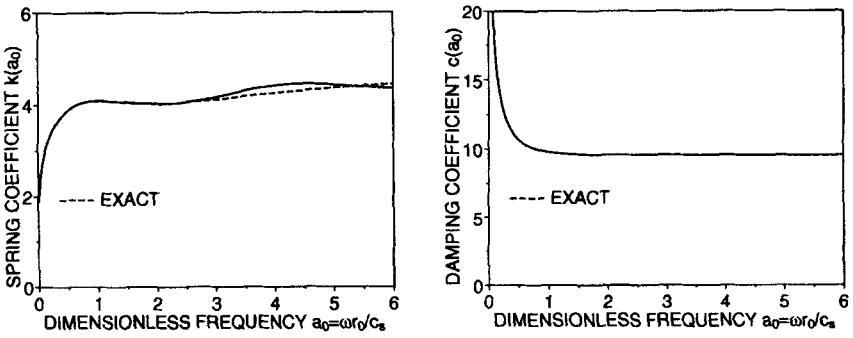

Figure 8. Dynamic-stiffness coefficient of circular cavity

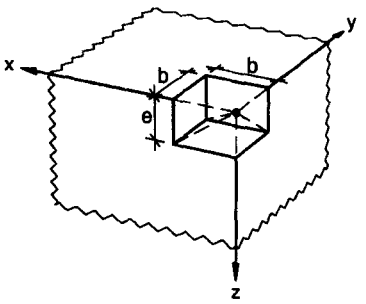

Figure 9. One quarter of square prism embedded in half-space

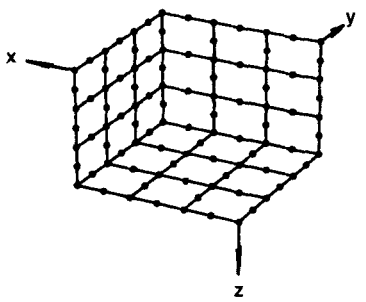

Figure 10. Finite-element mesh of one quarter of structure–medium interface of square prism

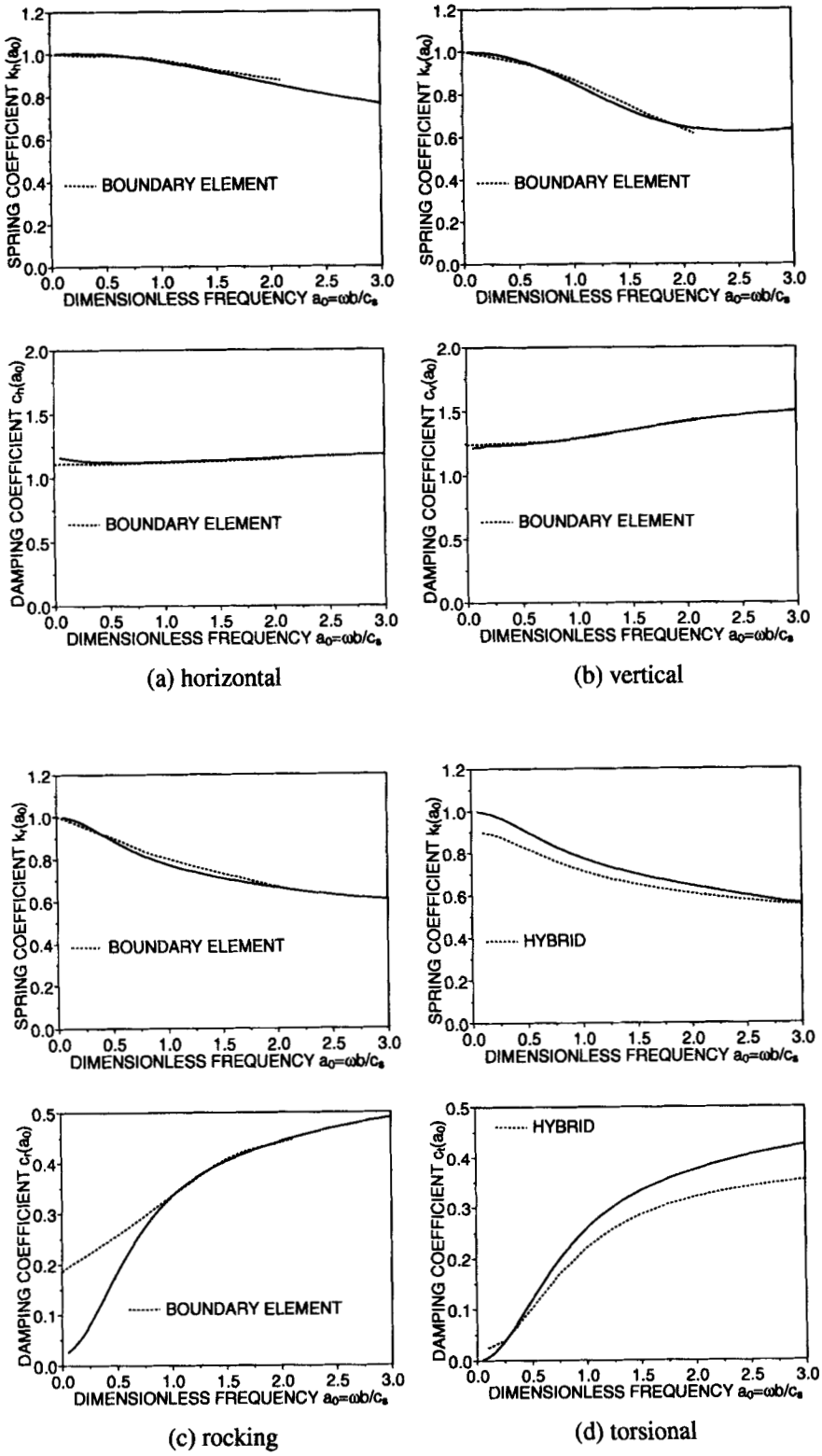

Figure 11. Dynamic-stiffness coefficients of rigid prism embedded in half-space

boundary condition $[S^{\infty}(\omega_h)]$ determined from the asymptotic expansion with $m = 2$ (equation (59)) at $\omega_h = a_{0h}c_s/r_0$ for $a_{0h} = 40$. A rigid interface is introduced. $\{\phi_h\}$, $\{\phi_v\}$, $\{\phi_r\}$ and $\{\phi_t\}$ correspond to the motion patterns of the nodes on the structure–medium interface associated with the horizontal, vertical, rocking and torsion motions, respectively. The dynamic-stiffness coefficients $S_h^{\infty}(\omega)$, $S_v^{\infty}(\omega)$, $S_r^{\infty}(\omega)$ and $S_t^{\infty}(\omega)$ are calculated from equation (95). After normalization with the static-stiffness coefficients a decomposition in the dimensionless spring coefficients and damping coefficients is performed as specified in equation (90). The dynamic-stiffness coefficients plotted in Figure 11 are compared with the results of the boundary-element method for the horizontal, vertical and rocking degrees of freedom in the frequency domain[8] and with those of the hybrid method for the torsional degree of freedom.[9]

6. CONCLUDING REMARKS

The consistent infinitesimal finite-element cell method to calculate the dynamic-stiffness matrix at the structure-medium interface of an unbounded medium is developed in the frequency domain. It is a stand-alone finite-element procedure. Only the structure–medium interface is discretized with the boundary condition at the free surface satisfied automatically. High accuracy results throughout the frequency range of interest.

REFERENCES

1. Ch. Song and J. P. Wolf, 'Consistent infinitesimal finite-element cell method: three-dimensional vector wave equation', *Int. j. numer. methods eng.* **39**, 2189–2208 (1996).
2. G. Waas, Linear two-dimensional analysis of soil dynamics problems in semi-infinite layered media, *Ph.D. Dissertation*, University of California, Berkeley, CA, 1972.
3. E. Kausel, J. M. Roësset and G. Waas, 'Dynamic analysis of footings on layered media', *J. eng. Mech. ASCE* **101**, 679–693 (1975).
4. W. H. Press, B. P. Flannery, S. A. Teukolsky and W. T. Vetterling, *Numerical Recipes*, Chapter 15, Cambridge University Press, Cambridge, 1988.
5. J. P. Wolf, *Soil–Structure-Interaction Analysis in Time Domain*, Prentice-Hall, Englewood Cliffs, NJ, 1988.
6. M. Novak, 'Dynamic stiffness and damping of piles', *Canadian geotech. j.* **11**, 574–598 (1974).
7. Y. Wang and R. K. N. D. Rajapakse, 'Dynamics of rigid strip foundations embedded in orthotropic elastic soils', *Earthquake eng. struct. dyn.* **20**, 927–947 (1991).
8. J. Dominguez, *Boundary Elements in Dynamics*, Computational Mechanics Publications, Southampton, 1993.
9. A. Mita and J. E. Luco, 'Impedance functions and input motions for embedded square foundations', *J. geotech. eng. ASCE* **115**, 491–503 (1989).